ELSEVIER

Image and Vision Computing 21 (2003) 205–220

image AND vision COMPUTING

www.elsevier.com/locate/imavis

Overall view regarding fundamental matrix estimation☆

Xavier Armangué, Joaquim Salvi*

Computer Vision and Robotics Group, Institute of Informatics and Applications, University of Girona, Avda. Lluís Santaló, s/n, E-17071 Girona, Spain

Received 26 September 2002; accepted 24 October 2002

Abstract

Epipolar geometry is a key point in computer vision and the fundamental matrix estimation is the only way to compute it. This article is a fresh look in the subject that overview classic and latest presented methods of fundamental matrix estimation which have been classified into linear methods, iterative methods and robust methods. All of these methods have been programmed and their accuracy analyzed in synthetic and real images. A summary including experimental results and algorithmic details is given and the whole code is available in Internet.

Keywords: Epipolar geometry; Fundamental matrix; Performance evaluation

1. Introduction

The estimation of three-dimensional (3D) information is a crucial problem in computer vision. At present, there are two approaches to accomplish this task. The first approach is based on a previous camera calibration. So that, the imaging sensor model that relates 3D object points to their 2D projections on the image plane is known. A thorough survey on camera modelling and calibration was presented by Ito in 1991 [1] and this subject has been widely studied during the last decades. Actually, basic methods model the imaging sensor through a single transformation matrix [2,3]. Other methods fix geometrical constraints in such matrix introducing a set of intrinsic and extrinsic camera parameters [4]. Moreover, lens distortion introduces two non-linear equations, which model the image curvature obtaining a more accurate model. Some authors have considered only radial lens distortion [5], while others considered tangential distortion [6], depending basically on the focal distance and lens curvature (see this camera calibration survey [7]). Finally, once the system is calibrated, the camera model can be used either to estimate the 2D projection of an object point or to compute the 3D optical ray passing through a given 2D image projection. Therefore, at least two optical rays are needed to compute the 3D position of the object point by means of triangulation.

Calibration cannot be used in active systems due to its lack of flexibility. Note that in active systems, the optical and geometrical characteristics of the cameras might change dynamically depending on the imaging scene and camera motion. The second approach then is based on computing either the epipolar geometry between both imaging sensors [8] or an Euclidean reconstruction [9]. Euclidean reconstruction is achieved through previous knowledge of the scene [10] such as projective basis and invariants. However, this assumption is difficult to integrate into many computer vision applications, while epipolar geometry is based only on image correspondences.

An application of scene reconstruction using Epipolar geometry was first published by Longuet-Higgins in 1981 [11]. Since that time, a great deal of effort has been done increasing the knowledge [8,12]. Many articles have been presented on self-calibrated and uncalibrated systems as a result of the boom in the 1990s. For instance, in 1992 Faugeras published a brief survey on self-calibration and the derived Kruppa equations which are used to estimate the camera parameters from the epipolar geometry [13]. Basically, intrinsic parameters of both cameras and the position and orientation of one camera related to the other can be extracted by using Kruppa equations [14]. In the same year, Faugeras also gave an answer to the question "What can be seen in three dimensions with an uncalibrated

☆ Work funded by Spanish project CICYT TAP99-0443-C05-01.
* Corresponding author. Tel.: +34-972-41-8483; fax: +34-972-41-8098.
E-mail addresses: qsalvi@eia.udg.es (J. Salvi), armangue@eia.udg.es (X. Armangué).

0262-8856/03/$ - see front matter
PII: S0262-8856(02)00154-3

stereo rig?" [15]. Hartley also did a lot of work with geometry and how it is contained in the essential and the fundamental matrix [16] as well as the estimation of the camera pose [17]. Two years later, Deriche et al. presented a robust method for recovering epipolar geometry based on a matching by correlation and detecting the outliers [18]. As a result, Hartley studied the geometry involved in a rotating camera [19] while Li studied the geometry of a head-eye system [20] and Luong et al. introduced a canonic representation [21]. Also, in 1994, Luong and Faugeras published an interesting article on analyzing the stability of the fundamental matrix due to uncertainty in the epipole computation, noise in the image point localization, camera motion, and so on [22].

Some applications of epipolar geometry are the simplification of the image matching in stereoscopic systems [23], the estimation of camera motion [24] and scene reconstruction [25]. It is important, therefore, to develop accurate techniques to compute it. Classic linear methods are mainly based on least-squares minimization [26] and eigen values minimization [27]. Other methods are based on optimizing linear methods by means of iteration [28]. Robust methods are based on computing a more accurate geometry detection and removing false matchings [26,29]. Robust computation is still a subject for wide research focusing mainly on proposing new estimators to improve the accuracy of the fundamental matrix and on reducing computation expenses [30–32].

This article surveys up to 19 of the most widely used techniques in computing the fundamental matrix such as the seven-point, least-squares and eigen analysis linear techniques among others and robust techniques such as M-Estimators, LMedS, RANSAC and so on. All these techniques have been programmed and their accuracy analyzed in synthetic and real scenarios. This article is divided as follows. First, a brief introduction to epipolar geometry is presented. Then, all the surveyed methods are described in Section 4 analyzing their advantages and drawbacks with respect to the previous methods, presenting an overview of every surveyed technique in terms of the algorithmic point of view. Section 5 deals with the experimental results obtained with both synthetic and real images including the obtained epipolar geometry. Finally, the article ends with conclusions.

2. Epipolar geometry

Given a 3D object point $M = ({}^{W}X, {}^{W}Y, {}^{W}Z, 1)^{\mathrm{T}}$ expressed with respect to a world coordinate system $\{W\}$, and its 2D projection on the image plane in pixels $m = ({}^{I}X, {}^{I}Y, 1)^{\mathrm{T}}$, both points are related to a projective transformation matrix as shown in Eq. (1),

$$sm = {}^{I}\mathbf{P}_{W} M \tag{1}$$

in which s is a scale factor and ${}^{I}\mathbf{P}_{W}$ is a 3×4 matrix, which can be decomposed as

$${}^{I}\mathbf{P}_{W} = {}^{I}\mathbf{A}_{C}\, {}^{C}\mathbf{K}_{W} \tag{2}$$

in which ${}^{I}\mathbf{A}_{C}$ is a 3×4 matrix relating the metric camera coordinate system located at the focal point O_C to the image coordinate system located at the top-left corner of the image plane in pixels, that is the optical and internal geometry of the camera. Moreover, ${}^{C}\mathbf{K}_{W}$ is a 4×4 matrix which relates the camera coordinate system $\{C\}$ to the world coordinate system $\{W\}$, that is the position and orientation of the camera in the scene.

$${}^{C}\mathbf{K}_{W} = \begin{pmatrix} {}^{C}\mathbf{R}_{W} & {}^{C}t_{W} \\ 0 & 1 \end{pmatrix} \tag{3}$$

Then, epipolar geometry defines the geometry between the two cameras creating a stereoscopic system or geometry between two different positions of a mobile camera. Given an object point M and its 2D projections m and m' on both image planes, the three points define a plane Π, which intersects both image planes at the epipolar lines $l_{m'}$ and l'_{m}, respectively, as shown in Fig. 1. Note that the same plane Π can be computed using both focal points O_C and $O_{C'}$ and a single 2D projection, which is the principle to reduce the correspondence problem to a single scanning along the epipolar line. Moreover, the intersection of all the epipolar lines defines an epipole on both image planes, which can also be obtained by intersecting the line defined by both focal points O_C and $O_{C'}$ with both image planes.

All the epipolar geometry is contained in the so called fundamental matrix as shown in Eq. (4).

$$m^{\mathrm{T}}\mathbf{F}m' = 0 \tag{4}$$

The fundamental matrix $\mathbf{F}$ contains the intrinsic parameters of both cameras and the rigid transformation of one camera related to the other, which depends on which camera has been considered as the origin of the world coordinate system. In Eq. (5), the origin of the world coordinate system coincides with the coordinate system of the second camera, located at $O_{C'}$.

$$\mathbf{F} = {}^{I}\mathbf{A}_{C}^{-\mathrm{T}} [{}^{C}t_{C'}] \times {}^{C}\mathbf{R}_{C'}\, {}^{I'}\mathbf{A}_{C'}^{-1} \tag{5}$$

A particular case of the fundamental matrix is the essential matrix. When the intrinsic camera parameters are known, it is possible to simplify Eqs. (4) and (5) obtaining

$$q^{\mathrm{T}}\mathbf{E}q' = 0 \tag{6}$$

where

$$q = {}^{I}\mathbf{A}_{C}^{-1} m, \qquad \mathbf{E} = [{}^{C}t_{C'}] \times {}^{C}\mathbf{R}_{C'}, \qquad q' = {}^{I'}\mathbf{A}_{C'}^{-1} m' \tag{7}$$

The matrix $\mathbf{E}$ is called essential [12].

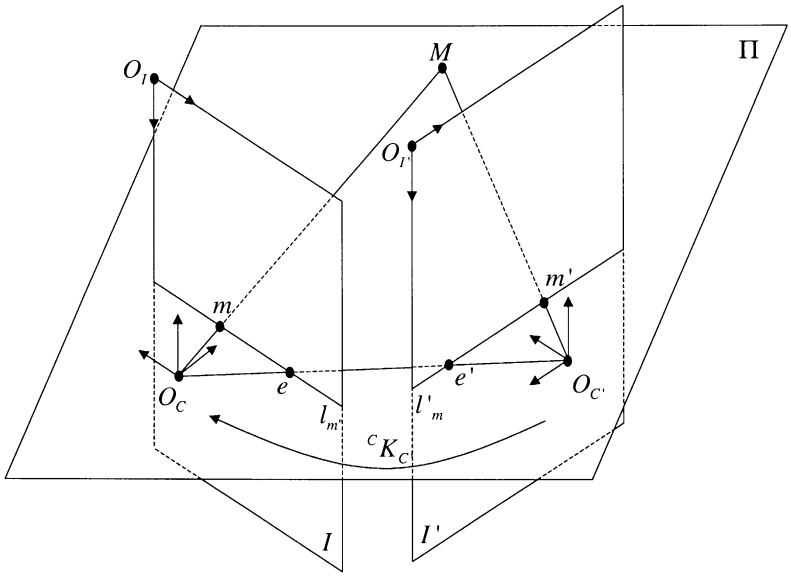

Fig. 1. The geometric relation between two pinhole cameras.

3. Estimating the fundamental matrix

In the last few years, several methods to estimate the fundamental matrix have been proposed, which can be classified into linear, iterative and robust methods. Linear and iterative methods can cope with bad point localization in the image plane due to noise in image segmentation. Robust methods can cope with both image noise and outliers, i.e. wrong matching between point correspondences in both image planes. All of these methods are based on solving a homogeneous system of equations which can be deduced from Eq. (4) rewriting it in the following way:

$$\mathbf{U}f = 0 \tag{8}$$

where

$$f = (F_{11}, F_{12}, F_{13}, F_{21}, F_{22}, F_{23}, F_{31}, F_{32}, F_{33})^{\mathrm{T}} \tag{9}$$

$$U = \begin{pmatrix} {}^{I}X_1\,{}^{I}X'_1 & {}^{I}X_1\,{}^{I}Y'_1 & {}^{I}X_1 & {}^{I}Y_1\,{}^{I}X'_1 & {}^{I}Y_1\,{}^{I}X'_1 & {}^{I}Y_1 & {}^{I}X'_1 & {}^{I}Y'_1 & 1 \\ \vdots & \vdots & \vdots & \vdots & \vdots & \vdots & \vdots & \vdots & \vdots \\ {}^{I}X_n\,{}^{I}X'_n & {}^{I}X_n\,{}^{I}Y'_n & {}^{I}X_n & {}^{I}Y_n\,{}^{I}X'_n & {}^{I}Y_n\,{}^{I}X'_n & {}^{I}Y_n & {}^{I}X'_n & {}^{I}Y'_n & 1 \end{pmatrix} \tag{10}$$

It is important to note that there are only seven independent parameters and nine unknowns. The seven independent parameters are given by two independent columns and the scale factor forcing the fundamental matrix to be rank-2 [26].

3.1. Linear methods

The linear method of the *seven points* is based on computing the fundamental matrix by using only seven point correspondences [26]. Due to the homogeneity of the equations, the solution is a set of matrices of the form

$$\mathbf{F} = \alpha\mathbf{F}_1 + (1-\alpha)\mathbf{F}_2 \tag{11}$$

By forcing the rank of the matrix to be equal to 2 and using the expression $\det[\alpha\mathbf{F}_1 + (1-\alpha)\mathbf{F}_2]$, a cubic polynomial is obtained which has to be solved to obtain α and then $\mathbf{F}$. The main advantage of this method is that a fundamental matrix can be estimated by using only seven points. However, this fact becomes a drawback when some points are poorly located. Moreover, the seven-points method cannot be applied in the presence of redundancy. Hence, it cannot be applied using n points where $n > 7$.

Another interesting method is the *eight-points method*, in which the redundancy of points permits the minimization of the error in estimating $\mathbf{F}$. The equation to minimize in the eight-points method is the residual of Eq. (4), that is:

$$\min_{\mathbf{F}} \sum_i (m_i^{\mathrm{T}}\mathbf{F}m'_i)^2 \tag{12}$$

The classical method to solve such an equation is the *least-squares technique* of forcing one of the components of $\mathbf{F}$ to be the unity [33]. This simplification can be assumed because $\mathbf{F}$ is always defined up to a scale factor. Then, the equation to solve is

$$f' = (\mathbf{U}'^{\mathrm{T}}\mathbf{U}')^{-1}\mathbf{U}'^{\mathrm{T}}c_9 \tag{13}$$

in which $\mathbf{U}'$ is a matrix containing the first eight columns of $\mathbf{U}$, c_9 is the last column of $\mathbf{U}$ (see also Eq. (10)) and f' is a vector containing the first eight elements of f. Note that the last element of f is 1.

A variant of the eight-points method can be applied if Eq. (12) is solved by using *eigen analysis*, also called *orthogonal least-squares technique* [27]. In this case $\mathbf{F}$ can

be determined from the eigen vector corresponding to the smallest eigen value of $\mathbf{U}^{\mathrm{T}}\mathbf{U}$. The difference between this method and the classical least-squares resides in the form of calculating the error between correspondences and epipolar lines so that an orthogonal minimization is much more realistic.

The last linear method we surveyed is the *analytic method with rank-2 constraint* which imposes the rank-2 constraint in minimization [26]. Then, the matrix $\mathbf{U}'$ is defined as the composition of the first seven columns of $\mathbf{U}$ and c_8 and c_9 are defined as the eighth and ninth columns of $\mathbf{U}$, respectively, so that $\mathbf{F}$ can be computed as

$$f' = -f_8(\mathbf{U}'^{\mathrm{T}}\mathbf{U}')^{-1}\mathbf{U}'^{\mathrm{T}}c_8 - f_9(\mathbf{U}'^{\mathrm{T}}\mathbf{U}')^{-1}\mathbf{U}'^{\mathrm{T}}c_9 \tag{14}$$

in which f' is the vector containing the first seven elements of f, and f_8 and f_9 are the eighth and ninth elements of f. In order to obtain the values of f_8 and f_9, $\mathbf{F}$ is computed by using the seven points algorithm. Then, f is computed by selecting from any choice of pairs of $\mathbf{F}$, the one which minimizes $\|f\| = 1$. Although the analytic method with rank-2 constraint obtains a rank-2 matrix, it does not greatly improve the results of the previously explained methods.

Concluding, the linear methods present an interesting reduced computing time (see Section 5) but their accuracy is rather poor in the presence of false matching or if the points are only badly located due to image noise. In order to obtain better results, iterative algorithms have to be considered.

3.2. Iterative methods

Iterative methods can be classified into two groups: those that minimize the distances between points and epipolar lines and those that are based on the gradient.

In the first classification, the iterative methods minimizing the distances between points and epipolar lines are based on solving the following equation

$$\min_{\mathbf{F}} \sum_i (d^2(m_i, \mathbf{F}m_i') + d^2(m_i', \mathbf{F}m_i)) \tag{15}$$

A first approach consists of directly applying an iterative method as *Newton–Raphson* or *Levenberg-Marquardt* in Eq. (15)[34]. Another possibility consists of applying an *iterative linear method* as was proposed by Luong and Faugeras (1993) [26], in which Eq. (15) has to be rewritten as

$$\min_{\mathbf{F}} \sum_i w_i^2 (m_i^{\mathrm{T}}\mathbf{F}m_i')^2 \tag{16}$$

where

$$w_i = \left(\frac{1}{l_1^2 + l_2^2} + \frac{1}{l_1'^2 + l_2'^2} \right)^{1/2} \tag{17}$$

$$\mathbf{F}m_i' = (l_1, l_2, l_3)^{\mathrm{T}} \tag{18}$$

$$\mathbf{F}^{\mathrm{T}}m_i = (l_1', l_2', l_3')^{\mathrm{T}} \tag{19}$$

The iterative linear method is based on computing the weight value w_i equivalent to the epipolar distances by using the previous $\mathbf{F}$ (in the first iteration $w_i = 1$) and then minimize by using *least-squares* in each iteration. Neither approach imposes the rank-2 constraint. However, the *non-linear minimization in parameter space* [26] can solve this situation. This method is based on parameterizing the fundamental matrix, keeping in mind that it has a rank-2 in the following way,

$$\mathbf{F} = \begin{pmatrix} a & b & -ax_e - by_e \\ c & d & -cx_e - dy_e \\ -ax_{e'} - cy_{e'} & -bx_{e'} - dy_{e'} & (ax_e + by_e)x_{e'} + (cx_e + dy_e)y_{e'} \end{pmatrix} \tag{20}$$

in which (x_e, y_e) and $(x_{e'}, y_{e'})$ are the coordinates of the epipole in the first image plane and second image plane, respectively. Eq. (20) is just one of the multiple parameterizations of $\mathbf{F}$ which must be computed. Finally, the estimated $\mathbf{F}$ becomes the parameterization which maximizes the following equation,

$$(ad - bc)^2 \sqrt{x_e^2 + y_e^2 + 1} \sqrt{x_{e'}^2 + y_{e'}^2 + 1} \tag{21}$$

The iteration of this method allows computing better rank-2 $\mathbf{F}$.

Besides, the minimization of Eq. (12) is not accurate enough to obtain a good estimation because the variance of points is not analogous and the least-squares technique assumes they are comparable. In order to overcome this drawback, the second group of methods has to be considered.

The second group of methods is based on the *gradient-based* [35]. In this case, the equation to solve is

$$\min_{\mathbf{F}} \sum_i (m_i^{\mathrm{T}}\mathbf{F}m_i')^2 / g_i^2 \tag{22}$$

where $g_i = \sqrt{l_1^2 + l_2^2 + l_1'^2 + l_2'^2}$.

This method has to potential minimizations: least-squares and eigen analysis. Besides, Chojnacki et al. [36] recently proposed two new iterative methods based on an approximate maximum likelihood estimate which can be applied to several computer vision applications. Such methods are called *Fundamental Numerical Scheme* (FNS) and *Constrained Fundamental Numerical Scheme* (CFNS). Both methods are based on Newton–Raphson minimization technique. Then, in order to estimate the fundamental matrix $\mathbf{F}$ the following minimization has to be overcome,

$$J_{\mathrm{AML}} = \sum_i \frac{(m_i^{\mathrm{T}}\mathbf{F}m_i')^2}{m_i^{\mathrm{T}}\mathbf{F}\mathbf{F}^{\mathrm{T}}m_i + m_i'^{\mathrm{T}}\mathbf{F}\mathbf{F}^{\mathrm{T}}m_i'} \tag{23}$$

so that $\partial_f J_{\mathrm{AML}}(f)$ is the row vector of partial derivatives of J_{AML} with respect to f. The minimization forces such vector to zero so that $\partial_f J_{\mathrm{AML}}(f) = 2\mathbf{X}_f f$. Then, arranging

the terms of this equation,

$$\mathbf{X}_f f = 0 \tag{24}$$

where

$$\mathbf{X}_f = \sum_{i=1}^{n} \frac{\mathbf{A}_i}{f^{\mathrm{T}}\mathbf{B}_i f} - \sum_{i=1}^{n} \frac{f^{\mathrm{T}}\mathbf{A}_i f}{(f^{\mathrm{T}}\mathbf{B}_i f)^2}\mathbf{B}_i \tag{25}$$

$$\mathbf{A}_i = u_i u_i^{\mathrm{T}} \tag{26}$$

$$\mathbf{B}_i = \partial_m u_i \Lambda_m \partial_m u_i^{\mathrm{T}} \tag{27}$$

∂_m represents the partial derivative of the corresponding points, Λ_m is the symmetric covariance matrix that relates the point uncertainty [37,38]. Then, FNS is based on solving Eq. (24) by means of an initial seed to search for an local minimum.

The CFNS [36] improves FNS by including in the optimization method an ancillary constraint obtained from the minimization function. In such a case, the $\mathbf{X}_f$ matrix is replaced to a more complex one, i.e. $\mathbf{Z}_f$.

$$\mathbf{Z}_f = \mathbf{P}_f \mathbf{X}_f \mathbf{P}_f \tag{28}$$

where

$$\mathbf{P}_f = \mathbf{I} - \|a_f\|^{-2} a_f a_f^{\mathrm{T}} \tag{29}$$

$$a_f = \partial_f \phi(f)^{\mathrm{T}} \tag{30}$$

and $\phi(f) = 0$ is the ancillary constraint.

The gradient-based technique obtains better results when compared with linear methods and iterative methods which minimize the distance between points and epipolar lines. Although iterative methods are more accurate than linear methods, they compute intensively and cannot cope with potential outliers.

3.3. Robust methods

In this section we present five robust methods: *M-Estimators*, *Least-Median-Squares* (LMedS), *Random Sampling* (RANSAC), MLESAC and MAPSAC which can be used both in the presence of outliers and in bad point localization.

M-Estimators [35] reduces the effect of outliers weighting the residual of each point. Consider r_i the residual of $m_i^{\mathrm{T}}\mathbf{F}m_i'$. Then, M-Estimators are based on solving the following expression

$$\min_{\mathbf{F}} \sum_i w_i (m_i^{\mathrm{T}}\mathbf{F}m_i')^2 \tag{31}$$

in which w_i is a weight function. A lot of different weight functions have been proposed so a new M-Estimator is obtained for each one. A common weight function proposed by Huber [39] is the following

$$w_i = \begin{cases} 1 & |r_i| \le \sigma \\ \sigma/|r_i| & \sigma < |r_i| \le 3\sigma \\ 0 & 3\sigma < |r_i| \end{cases} \tag{32}$$

Another interesting weight function is proposed by Turkey [40],

$$w_i = \begin{cases} \left(1 - \left(\frac{r_i}{4.6851}\right)^2\right)^2 & |r_i| \le 4.6851\sigma \\ 0 & \text{otherwise} \end{cases} \tag{33}$$

In order to obtain σ, the robust standard deviation can be used (see Ref. [26]).

$$\sigma = 1.4826(1 + 5/(n-7))\text{median}_i|r_i| \tag{34}$$

There are a lot of weight functions and for each one we obtained different results. The results given by this method are quite good in the presence of gaussian noise in image point localization, but they are rather limited in outlier detection.

LMedS [26] and *RANSAC* [27] techniques are quite similar. Both techniques are based on randomly selecting the set of points used to compute an approximation of **F** by using a linear method. The difference between both techniques is in the way use to determine the chosen **F**. LMedS calculates for each **F** the median distance between the points and epipolar lines, in which the chosen fundamental matrix has to minimize this median. RANSAC calculates for each **F** the number of inliers, in which the chosen **F** is the one that maximizes it. Once the outliers are removed, **F** is recalculated with the aim of obtaining a better approach.

Another difference between both methods is that LMedS is more restrictive than RANSAC, so that LMedS removes more points than RANSAC. However, the principal constraints of both techniques are their lack of repetitivity due to the aleatory way of selecting the points. Although experimental results show that LMedS gives better results in terms of accuracy, it does not always model the epipolar geometry properly.

Recently some other methods based on RANSAC has been proposed. The MLESAC [32] (*Maximum LikElihood SAmple Consensus*) is a generalization of RANSAC based on the same point selection strategy and the solution is the one that maximizes a likelihood, so that the shape of a normal distribution instead of the number of inliers. Besides, MAPSAC [41] (*Maximum A Posteriori SAmple Consensus*) improves MLESAC being more robust against noise and outliers including Bayesian probabilities in minimization.

3.4. Algorithmic overview

This section gives an algorithmic point of view of the surveyed methods to estimate the fundamental matrix

described in Sections 4.1–4.3. The main objective of this section is to present an overall schema to make agile the comparison among the different methodologies.

Fig. 2 summarizes the algorithmic methodology of the linear methods. Besides, Fig. 3 abstracts the methodology used by the iterative methods to minimize the distance between points and the corresponding epipolar lines. Moreover, Fig. 4 illustrates the schema of the iterative methods based on minimizing the gradient and the approximate maximum likelihood. The two foremost schemas are two different implementations of the gradient technique, that is, linear-squares and eigen analysis. The two aftermost schemas are based on FNS and CFNS which methodology are quite similar. Note that $\mathbf{Z}_f = 0$ is equivalent to $\mathbf{Z}_f^{\mathrm{T}}\mathbf{Z}_f = 0$ obtaining a symmetric matrix which is replaced to $\mathbf{X}_f$ in the algorithm. Finally, Fig. 5 deals with robust methods. The first schemas are three different implementations of the M-Estimator technique, that is the minimization of Eq. (31) by using least-squares and eigen analysis, and the implementation proposed by Torr [27] in which the fundamental matrix is forced to be rank-2 in every iteration (explained in detail in Section 4.5.2). The last methods shown in Fig. 5 correspond to LMedS and RANSAC, respectively.

3.5. Considerations in *F* estimation

3.5.1. Normalizing data

Data normalization is a key point in fundamental matrix estimation. It has been proved that the computation should not be applied directly to raw data in pixels due to potential uncertainties given by huge numbers. The process of normalization consists of scaling and translating the data so that points m_i and m_i' are transformed to ($\hat{m}_i = \mathbf{T}m_i$ and $\hat{m}_i' = \mathbf{T}'m_i'$) by using two transformation matrices $\mathbf{T}$ and $\mathbf{T}'$, respectively. Then, the $\hat{\mathbf{F}}$ matrix is estimated from the normalized points and, finally, it has to be restored to obtain $\mathbf{F}$ using the following equation

$$\mathbf{F} = \mathbf{T}^{\mathrm{T}}\hat{\mathbf{F}}\mathbf{T}' \tag{35}$$

Basically there are two different methods of data normalization. The first method [26] normalizes the data between $[-1,1]$. The second was proposed by Hartley [42] and is based on two transformations. First, the points are translated so that their centroid is placed at the origin. Then, the points are scaled so that the mean of the distances of the points to the origin is $\sqrt{2}$. It has been proved that Hartley's method gives more accurate results than normalizing between $[-1,1]$.

3.5.2. Rank-2 constraint

In most circumstances, the estimated $\mathbf{F}$ should be a rank-2 matrix in order to model the epipolar geometry with all the epipolar lines intersecting in a unique epipole. Although the rank-2 constraint is not imposed in most of the surveyed methods, there is a mathematical method which transforms a rank-n square matrix to the closest rank-$(n-1)$ matrix [35]. The $\mathbf{F}$ is decomposed in

$$\mathbf{F} = \mathbf{U}\mathbf{S}\mathbf{V}^{\mathrm{T}} \tag{36}$$

by using singular value decomposition, where $\hat{\mathbf{S}} = \mathrm{diag}(\sqrt{\lambda_1}, \sqrt{\lambda_2}, \sqrt{\lambda_3})$. The component with the smallest weight is removed obtaining $\hat{\mathbf{S}} = \mathrm{diag}(\sqrt{\lambda_1}, \sqrt{\lambda_2}, 0)$. Then, $\mathbf{F}$ is recalculated in the following way:

$$\hat{\mathbf{F}} = \mathbf{U}\hat{\mathbf{S}}\mathbf{V}^{\mathrm{T}} \tag{37}$$

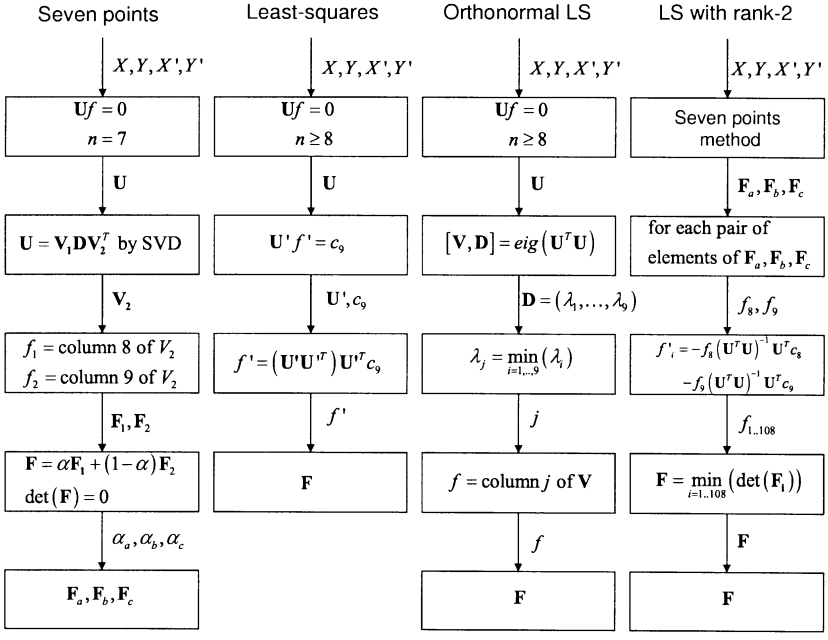

Fig. 2. Linear methods flow schemes.

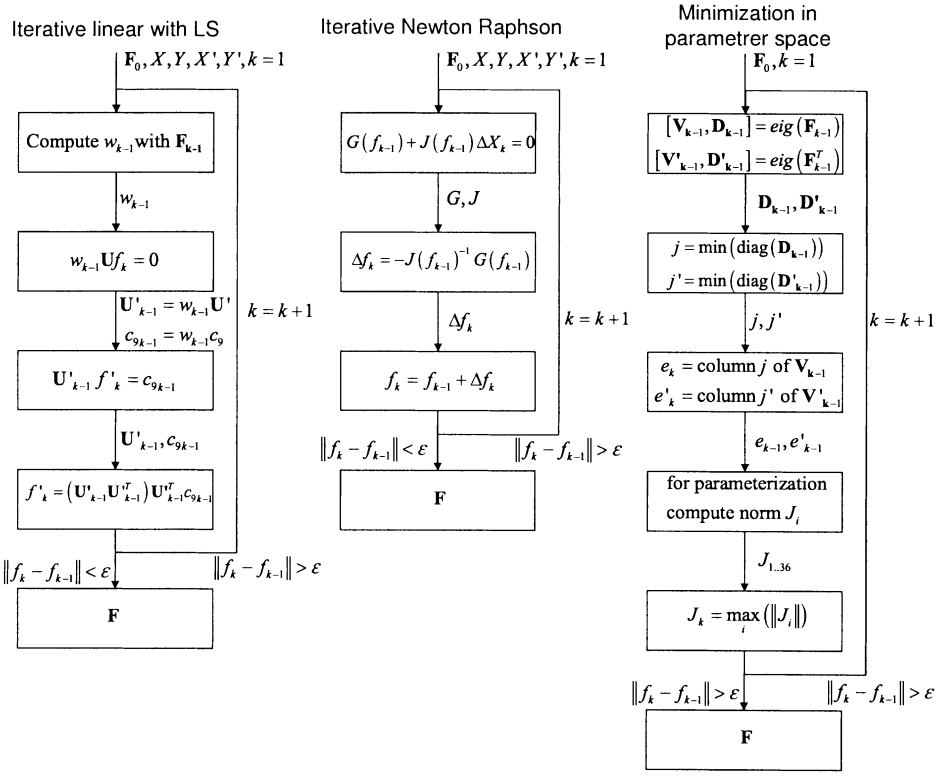

Fig. 3. Flow schemes of the iterative methods minimizing the distances between points and epipolar lines.

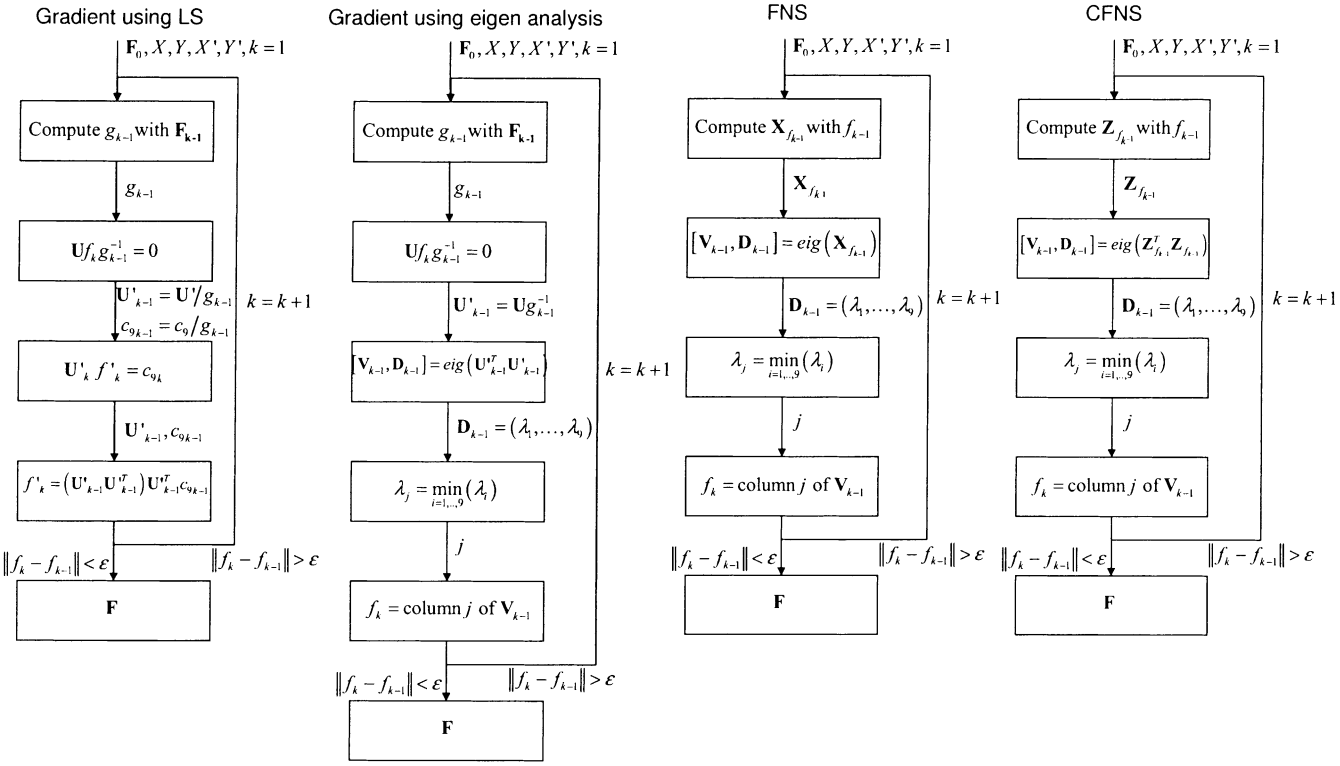

Fig. 4. Flow schemes of the iterative methods minimizing the gradient.

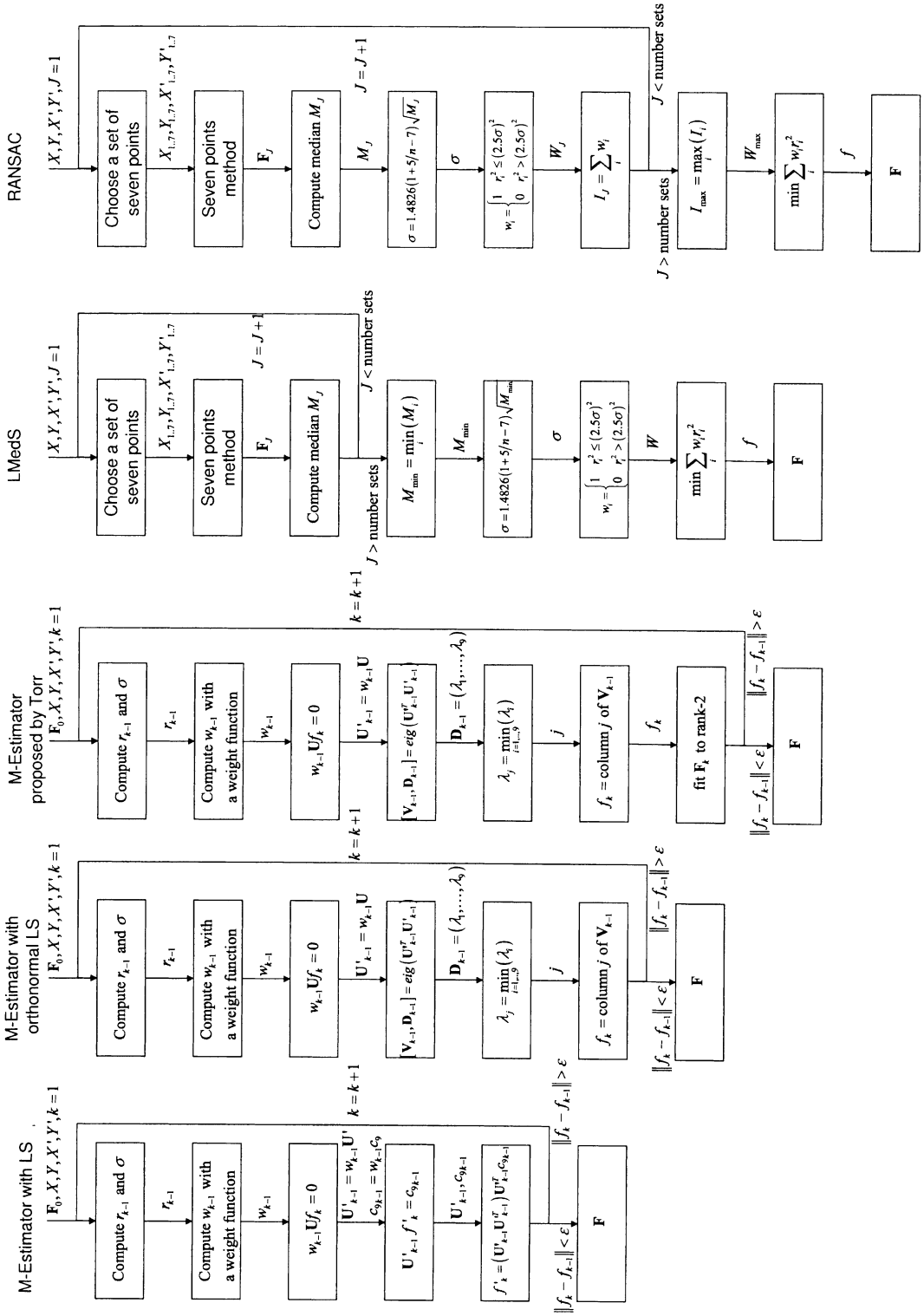

Fig. 5. Flow schemes of M-Estimators, LMedS and RANSAC methods.

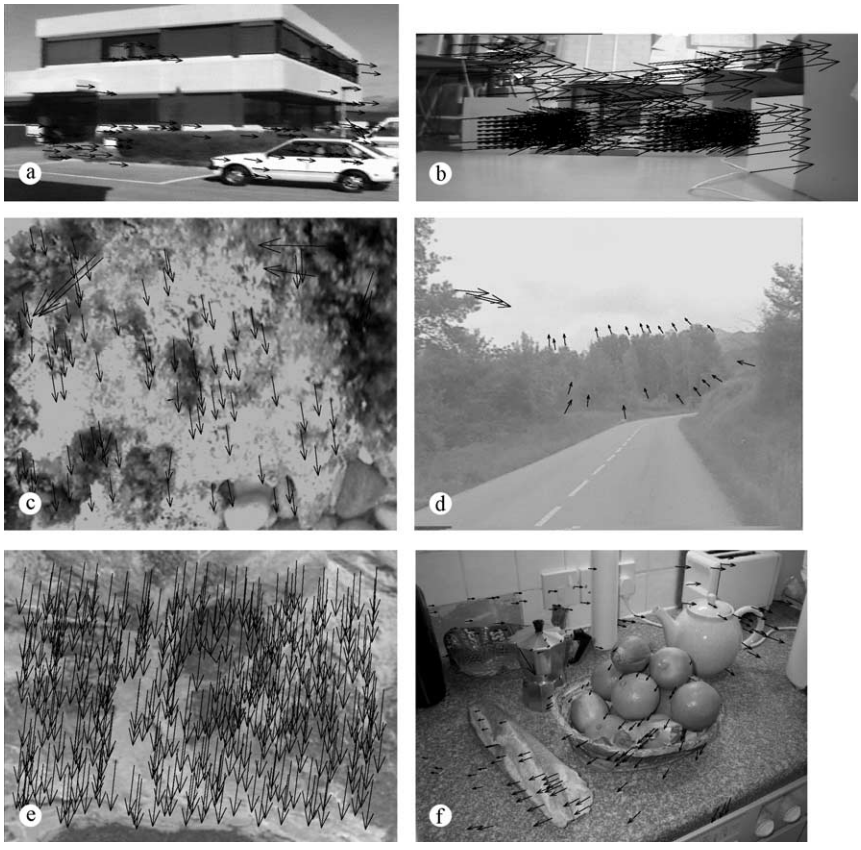

Fig. 6. Correspondences used in real images: (a) urban scene; (b) mobile robot scene; (c) underwater scene; (d) road scene; (e) aerial scene; (f) kitchen scene.

However, transforming the obtained **F** to a rank-2 matrix will give worse results because the obtained optimized matrix is rank-3. Besides, a rank-3 matrix gives an additional degree of freedom that usually reduces the distance between points and epipolar lines.

Overall, we suggest the use of any method which imposes a rank-2 matrix in the computation of **F** because rank-2 matrices models more accurate the epipolar geometry.

4. Experimental results

The surveyed methods have been programmed[1] and their accuracy analyzed with synthetic images varying the gaussian noise and the number of outliers. Moreover, the surveyed methods have been tested by using real images in different scenarios, that is urban scenes, mobile robot indoor environment, seabed, road images, aerial and images of a potential kitchen. The correspondence problem between images have been solved by using the algorithm proposed by Zhang[2] [43] and the obtained results are shown in Fig. 6. The corresponding points have normalized by the method proposed by Hartley [42] described in Section 4.5.1.

[1] FNS, CFNS, MLESAC and MAPSAC implementations have been provided by the original authors.

[2] Available at http://www-sop.inria.fr/robotvis/demo/f-http/html.

Table 1 shows the accuracy of each method computed as the mean and standard deviation of the distances between points and epipolar lines.

The seven points algorithm obtains a solution using only seven points. However, the accuracy depends greatly on the points used. The least-squares technique is based on using at least eight points and its accuracy depends on the amount of badly located points used, usually obtaining better results by increasing the amount of points. The eigen analysis is the linear method that obtains the best results because an orthogonal least-squares minimization is more realistic than the classic one. However, all these methods obtain a rank-3 fundamental matrix, which means that the epipolar geometry is not properly modeled. The analytic method with rank-2 constraint obtains a rank-2 fundamental matrix in which distances between points and epipolar lines are worse than in the linear methods and it is more expansive in computing time (see Fig. 7).

The iterative linear method improves considerably the least-squares technique but cannot cope with outliers. The *iterative Newton–Raphson algorithm* gets even better results than the previous method if the presence of outliers is not considered. Although the *non-linear minimization in parameter space* also obtains a rank-2 matrix, the distances of points to epipolar lines are the worst and sometimes the method diverges obtaining a false solution. The eighth and

Table 1
Synthetic and real image results of methods. Every cell show the mean and standard deviation of the discrepancy between points and epipolar lines

Methods	Linear				Iterative							Robust							
	1	2	3	4	5	6	7	8	9	10	11	12	13	14	15	16	17	18	19
$\sigma = 0.0$ outliers 0%	14.250	0.000	0.000	1.920	0.000	0.000	0.000	0.000	0.000	0.000	0.000	0.000	0.000	0.000	0.000	0.000	0.000	0.100	0.011
	13.840	0.000	0.000	1.143	0.000	0.000	0.000	0.000	0.000	0.000	0.000	0.000	0.000	0.000	0.000	0.000	0.000	0.079	0.009
$\sigma = 0.0$ outliers 10%	25.370	339.562	17.124	30.027	161.684	20.445	Infty	187.474	18.224	17.124	16.978	273.403	4.909	4.714	0.000	0.000	16.457	19.375	0.115
	48.428	433.013	31.204	59.471	117.494	30.487	Infty	197.049	36.141	31.204	29.015	360.443	4.493	2.994	0.000	0.000	26.923	70.160	0.115
$\sigma = 0.1$ outliers 0%	135.775	1.331	0.107	0.120	1.328	0.107	1.641	1.328	0.112	0.107	0.110	0.355	0.062	0.062	1.331	0.107	0.107	0.139	0.168
	104.671	0.788	0.088	0.091	0.786	0.088	0.854	0.786	0.092	0.088	0.091	0.257	0.042	0.041	0.788	0.088	0.088	0.123	0.155
$\sigma = 0.1$ outliers 10%	140.637	476.841	19.675	70.053	158.961	32.765	146.955	183.961	15.807	14.003	14.897	73.354	4.876	4.130	0.449	0.098	2.389	21.784	0.701
	104.385	762.756	46.505	63.974	124.202	67.308	94.323	137.294	40.301	38.485	39.388	59.072	4.808	2.997	0.271	0.077	5.763	97.396	0.740
$\sigma = 0.5$ outliers 0%	163.839	5.548	0.538	0.642	5.599	0.538	7.017	5.590	0.554	0.538	0.543	2.062	0.392	0.367	5.548	0.538	0.538	0.550	0.762
	178.222	3.386	0.362	0.528	3.416	0.361	3.713	3.410	0.361	0.362	0.368	1.466	0.237	0.207	3.386	0.362	0.362	0.377	0.618
$\sigma = 0.5$ outliers 10%	140.932	507.653	19.262	26.475	161.210	31.740	Infty	217.577	19.409	22.302	22.262	143.442	3.887	3.147	47.418	0.586	18.942	23.859	0.629
	109.427	1340.808	49.243	54.067	136.828	59.126	Infty	368.061	51.154	59.048	59.162	111.694	3.969	2.883	29.912	0.434	53.098	79.890	0.452
$\sigma = 1.0$ outliers 0%	65.121	21.275	1.065	1.319	20.757	1.068	345.123	21.234	1.071	1.065	1.066	8.538	0.794	0.814	21.275	1.065	1.065	1.089	1.072
	58.184	12.747	0.744	0.912	12.467	0.772	294.176	12.719	0.745	0.744	0.748	6.306	0.463	0.463	12.747	0.744	0.744	0.768	0.785
$\sigma = 1.0$ outliers 10%	128.919	429.326	21.264	61.206	158.849	37.480	∞	152.906	18.730	18.374	19.683	120.012	3.921	4.089	25.759	1.052	14.076	19.298	1.041
	100.005	633.019	53.481	64.583	120.461	52.762	∞	120.827	38.644	39.993	42.112	122.436	3.752	4.326	15.217	0.803	30.274	65.149	0.822
Urban scene	51.633	1.724	0.440	1.023	1.102	0.468	2.974	1.109	0.446	0.437	0.437	1.668	0.309	0.279	1.724	0.319	0.440	0.449	0.440
	35.724	1.159	0.334	1.012	0.796	0.341	3.066	0.803	0.368	0.333	0.334	0.935	0.228	0.189	1.159	0.269	0.334	0.373	0.348
Mobile robot scene	119.439	35.525	4.080	16.511	46.216	5.611	24.010	18.665	4.787	4.080	3.199	5.775	0.274	0.593	24.835	1.559	3.855	2.443	1.274
	46.268	64.175	7.684	18.964	35.011	8.729	22.270	22.170	9.255	7.684	5.541	50.701	0.192	0.524	38.434	2.715	6.141	5.629	2.036
Underwater scene	97.977	4.683	1.725	5.242	3.068	1.752	5.575	2.949	1.581	1.599	1.609	0.557	0.650	0.475	2.439	0.847	1.725	3.678	1.000
	66.223	3.941	2.138	4.286	2.804	2.249	4.337	2.798	2.056	2.019	2.010	0.441	0.629	0.368	2.205	0.740	2.138	12.662	0.761
Road scene	27.668	0.825	0.609	1.078	0.511	0.559	1.920	0.512	0.809	0.466	0.595	0.373	0.136	0.310	0.825	0.609	0.609	0.427	0.471
	39.688	1.144	0.734	2.118	0.422	0.709	2.498	0.427	0.986	0.419	0.543	0.635	0.113	0.256	1.144	0.734	0.734	0.410	0.403
Aerial scene	99.635	0.179	0.149	1.480	0.179	0.149	0.497	0.179	0.342	0.149	0.209	0.099	0.085	0.161	0.179	0.149	0.149	0.216	0.257
	62.162	0.158	0.142	0.979	0.158	0.143	0.472	0.158	0.339	0.142	0.178	0.063	0.058	0.106	0.158	0.142	0.142	0.186	0.197
Kitchen scene	16.956	5.014	2.623	2.681	3.217	2.966	7.563	3.176	1.901	2.623	1.892	0.584	0.280	0.263	1.350	0.545	2.623	0.864	0.582
	16.696	5.177	3.327	4.175	2.476	3.310	5.576	2.508	1.499	3.327	2.504	0.425	0.207	0.191	1.200	0.686	3.327	3.713	0.717

Methods: (1) seven points; (2) least-squares (LS); (3) orthogonal LS; (4) rank-2 constraint; (5) iterative linear; (6) iterative Newton–Raphson; (7) minimization in parameter space; (8) gradient using LS; (9) gradient using eigen; (10) FNS; (11) CFNS; (12) M-Estimator using LS; (13) M-Estimator using eigen; (14) M-Estimator proposed by Torr; (15) LMedS using LS; (16) LMedS using eigen; (17) RANSAC; (18) MLESAC; (19) MAPSAC.

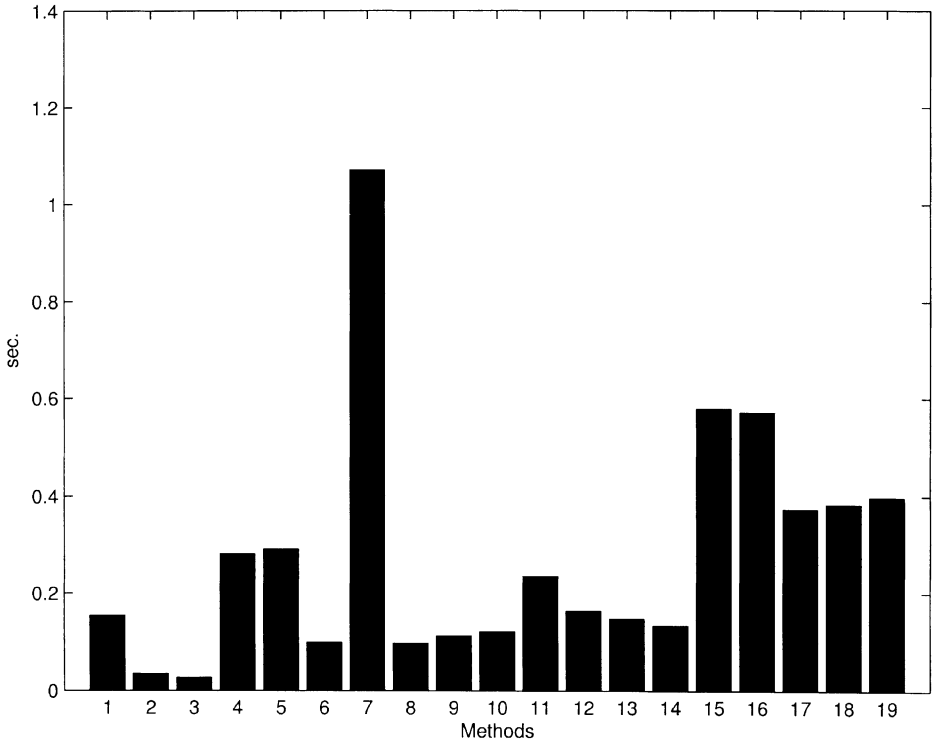

Fig. 7. Computing time of methods: (1) seven points; (2) least-squares (LS); (3) orthogonal LS; (4) rank-2 constraint; (5) iterative linear; (6) iterative Newton–Raphson; (7) minimization in parameter space; (8) gradient using LS; (9) gradient using eigen; (10) FNS; (11) CFNS; (12) M-Estimator using LS; (13) M-Estimator using eigen; (14) M-Estimator proposed by Torr; (15) LMedS using LS; (16) LMedS using eigen; (17) RANSAC; (18) MLESAC; (19) MAPSAC.

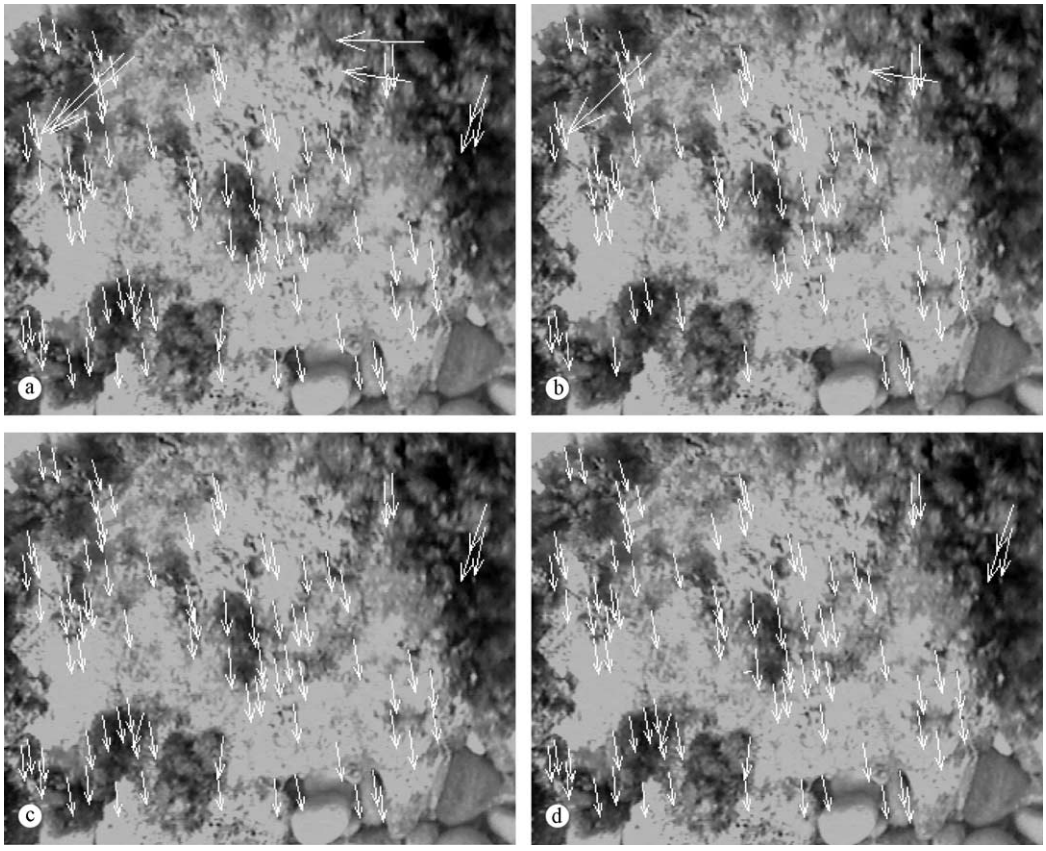

Fig. 8. Underwater scene and matchings: (a) set of initial correspondences; and the matchings kept by: (b) M-Estimators; (c) LMedS; (d) RANSAC.

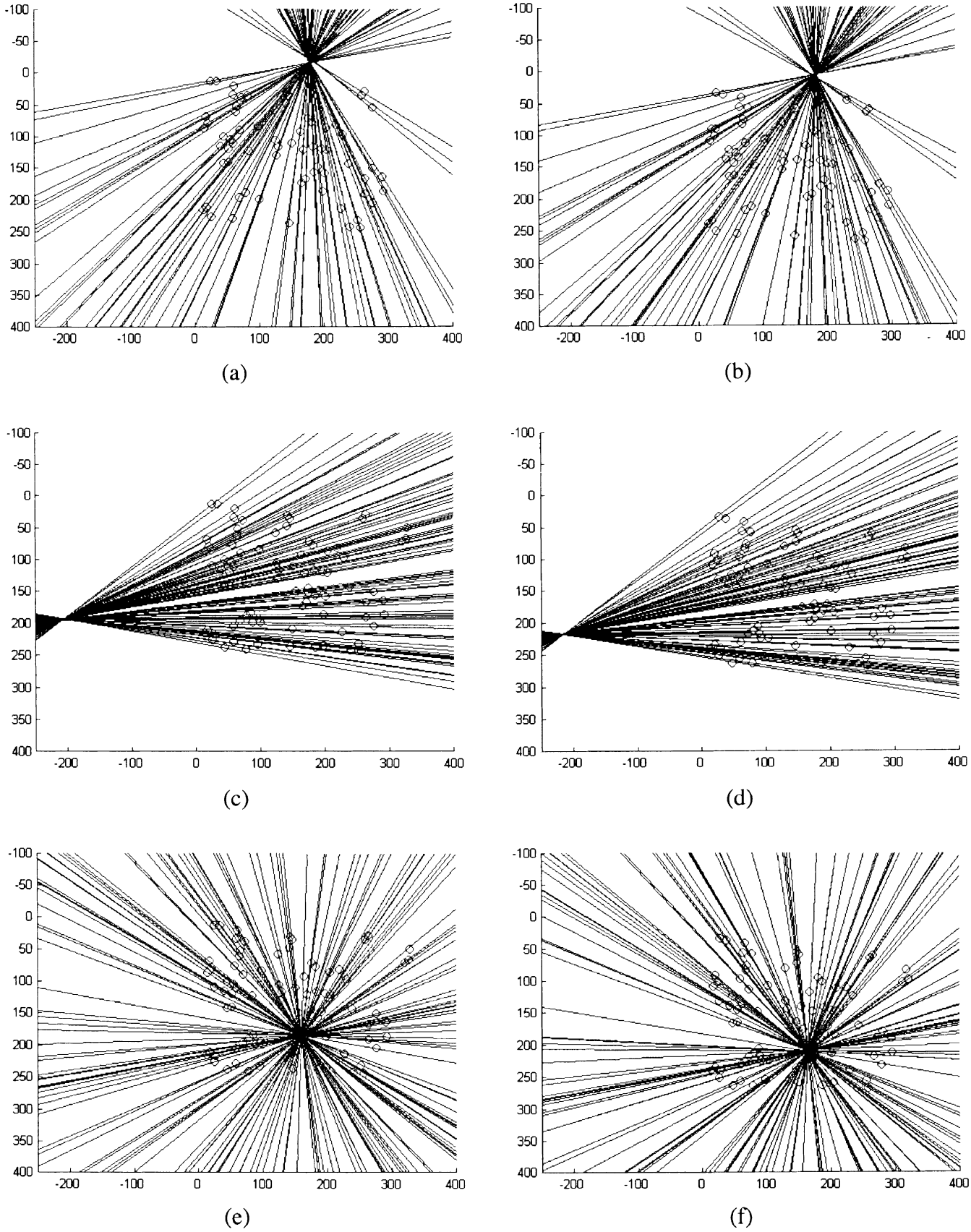

Fig. 9. Points and epipolar lines in the underwater scene: (a) left and (b) right views obtained by M-Estimator; (c) left and (d) right views obtained by LMedS; (e) left and (f) right views obtained by RANSAC.

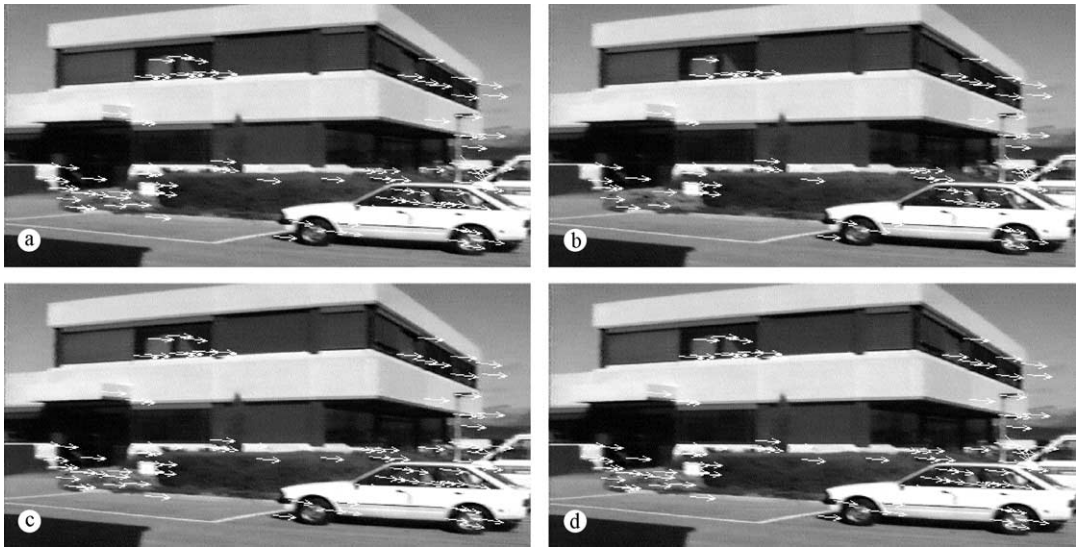

Fig. 10. Urban scene and matchings: (a) set of initial correspondences; and the matchings kept by: (b) M-Estimators; (c) LMedS; (d) RANSAC.

ninth methods are two different versions of the *gradient-based method* using least-squares and orthogonal least-squares, respectively. Both methods obtain better results than their equivalent linear methods. Nevertheless, the eigen analysis once more obtains better results than the other linear methods. Results obtained and computing time spent by the method *FNS* are quite similar to the gradient technique. Besides, *CFNS* improve slightly the results obtained by FNS spending more computing time, though. Summarizing, iterative methods improve the computation of the fundamental matrix but they cannot cope with outliers.

The last surveyed methods are classified into robust (see in Table 1 columns 12–19), which means that they might detect and remove potential outliers and compute the fundamental matrix by using only inliers. Three versions of the M-Estimators based on the Huber weight function have been programmed: least-squares, eigen analysis and the method proposed by Torr [27]. The three methods start from a linear initial guess and become fully dependent on the linear method used to estimate it. Moreover, least-squares and eigen values get a rank-3 matrix, while Torr forces a rank-2 matrix in each iteration giving a more accurate geometry. Besides, two different versions of LMedS using again least-squares and eigen analysis have been studied. Although the accuracy of LMedS seems worse compared to M-Estimators, LMedS removes the outliers more efficiently so that the epipolar geometry is properly obtained. RANSAC is the last surveyed method. However, RANSAC does not obtains any better results than LMedS with eigen analysis due to the method used to select the outliers which is quite permissive. MLESAC is a generalization of RANSAC obtaining more or less the same results. Besides, *MAPSAC* improves considerably the results obtained by RANSAC but MAPSAC does not improve the results obtained by LMedS.

Fig. 7 shows the mean computing time spent by the whole methods in synthetic and real scenarios. On the whole, computing time is linear dependent to complexity of the algorithm. So, least-squares turn out to be the quickest linear method, while Newton–Raphson and gradient techniques are the quickest iterative methods. Summarizing the robust methods, M-Estimators are quicker than the methods in which a set of points have to be selected aleatory from the images.

Fig. 8(a) shows the matchings obtained by using the method proposed by Zhang [43,44]. First, a Harris corner detector is applied to get a list of interesting points. Then the matching between both images is computed by using a pixel-based correlation. Note that matches might not be unique. Finally, a relaxation method is used to improve the local consistency of matches, reducing their ambiguity.

Fig. 8(b) shows the list of matchings kept by M-Estimator based on eigen values. Depending on the weighting function, the removed matchings vary due to both noise and outliers. Note that some good matchings are also removed while potential outliers are kept as inliers. Fig. 8(c) shows the results obtained by LMedS, while Fig. 8(d) shows the results obtained by RANSAC. In both cases, every single outlier is detected and removed, obtaining comparatively the same results.

Also, the geometry modeled by every robust method is quite different. Fig. 9(a) and (b) shows the epipolar geometry given by M-Estimator based on eigen values, wherein it is shown how the epipolar lines do not cross in a single epipole due to the rank-3 matrix obtained. LMedS obtains a completely different geometry in which epipoles have been located outside the image plane, but they are unique (see Fig. 9(c) and (d)). RANSAC obtains a geometry with the epipole located near the image center. Comparing the obtained geometries related to the position of the camera

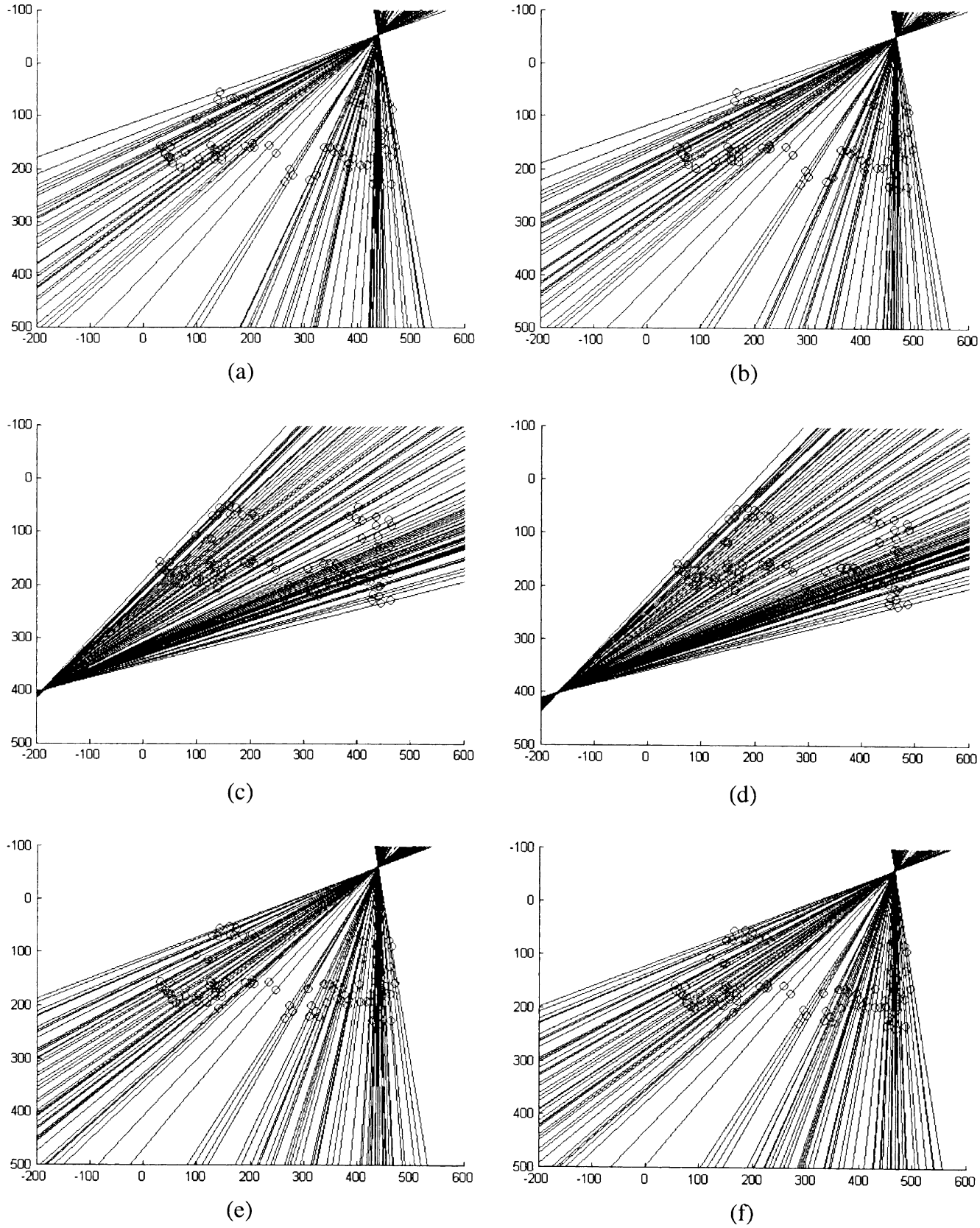

Fig. 11. Points and epipolar lines in the urban scene: (a) left and (b) right views obtained by M-Estimator; (c) left and (d) right views obtained by LMedS; (e) left and (f) right views obtained by RANSAC.

and its motion, the geometry modeled by RANSAC is the closest to reality.

The same study has been done considering the urban scene showing that the obtained results are a bit different. The reader can see these results in Figs. 10 and 11. The number of potential outliers is fewer than in the underwater scene and the location of image points is more accurate because of better image quality (see Fig. 10 (a) and (b) shows the poor results obtained by the eigen value M-Estimator, in which a lot of matchings are removed while some of the outliers are kept. In this case, LMedS is the only method, which detects the set of outliers located in the right side of the image (see Fig. 10(c)). Besides, RANSAC does not detect any outlier so results are not accurate enough.

The geometry obtained in the urban scene largely depends on the method utilized. Fig. 11 shows the three different geometries given by M-Estimator, LMedS and RANSAC. In this case, M-Estimator and RANSAC model a similar geometry in which the epipoles are located outside the image near the top-right corner, which is not the right situation. LMedS obtains the right geometry with the epipoles located in the left side of the image.

5. Conclusions

This article surveys up to 19 of the most used methods in fundamental matrix estimation. The different methods have been programmed and their accuracy analyzed in synthetic and real images. The methodology used has been compared and a useful overall schema is presented. Experimental results show that: (a) linear methods are quite good if the points are well located in the image and the corresponding problem previously solved; (b) iterative methods can cope with some gaussian noise in the localization of points, but they become really inefficient in the presence of outliers; (c) robust methods can cope with both discrepancy in the localization of points and false matchings.

Experimental results show that the orthogonal least-squares using eigen analysis gives better results than the classic least-squares technique of minimization. Moreover, a rank-2 method is preferred because it models the epipolar geometry with all the epipolar lines intersecting at a single epipole. Moreover, experimental results show that the corresponding points have to be normalized and the best results have been obtained by using the method proposed by Hartley [35]. Summarizing, the recently proposed method of MAPSAC obtains quite a good results with a low computing time. However, LMedS still obtain the best results when a low computing time is not required.

The uncertainty in fundamental matrix computation was studied in detail by Csurka et al. [45] and Torr and Zisserman [46]. The surveyed methods model the epipolar geometry without considering lens distortion, which considerably influences their discrepancy. Thus, some efforts have been made recently in presence of radial lens distortion [47]. In all, LMedS is the most appropriate for outlier detection and removal. However, with the aim of obtaining an accurate geometry, it is better to combine it with M-Estimator, which in our case has modeled a proper geometry in synthetic data, either in the presence of noise or outliers.

6. Software

A Matlab Toolkit illustrating all the surveyed methods is available, please check http://eia.udg.es/~armangue/research.

Acknowledgements

We greatly appreciate Dr W. Chojnacki and Dr A. van den Hengel who gave us insightful information and the code of their methods (FNS and CFNS), as well as Dr P.H.S. Torr who left the implementation of the MAPSAC and MLESAC methods in its web page. Finally, we thank Dr Z. Zhang for the implementation of the correspondence problem solution.

References

[1] M. Ito, Robot vision modelling—camera modelling and camera calibration, Advanced Robotics 5 (3) (1991) 321–335.
[2] P.I.J. Batlle, E. Mouaddib, J. Salvi, A survey: recent progress in coded structured light as a technique to solve the correspondence problem, International Journal of Pattern Recognition 31 (7) (1998) 963–982.
[3] E.L. Hall, J.B.K. Tio, C.A. McPherson, F.A. Sadjadi, Measuring curved surfaces for robot vision, Computer Journal 15 (12) (1982) 42–54.
[4] O.D. Faugeras, G. Toscani, The Calibration Problem for Stereo, Proceedings of the IEEE Conference on Computer Vision and Pattern Recognition, Los Alamitos, CA, 1986, pp. 15–20.
[5] R.Y. Tsai, A versatile camera calibration technique for high-accuracy 3D machine vision metrology using off-the-shelf TV cameras and lenses, IEEE International Journal on Robotics and Automation RA-3 (4) (1987) 323–344.
[6] J. Weng, P. Cohen, M. Herniou, Camera calibration with distortion models and accuracy evaluation, IEEE Transactions on Pattern Analysis and Machine Intelligence 14 (10) (1992) 965–980.
[7] J. Salvi, X. Armangué, J. Batlle, A comparative review of camera calibrating methods with accuracy evaluation, Pattern Recognition 35 (7) (2002) 1617–1635.
[8] O.D. Faugeras, Three-Dimensional Computer Vision, The MIT Press, Cambridge, MA, 1993.
[9] R.I. Hartley, Euclidean reconstruction from uncalibrated views, Second European Workshop on Applications of Invariance in Computer Vision (1993) 237–257.
[10] R. Mohr, E. Arbogast, It can be done without camera calibration, International Journal of Pattern Recognition Letters 12 (1991) 39–43.
[11] H.C. Longuet-Higgins, A computer algorithm for reconstructing a scene from two projections, Nature 293 (1981) 133–135.
[12] T.S. Huang, O.D. Faugeras, Some proprieties of the E matrix in two-view motion estimation, IEEE Transactions on Pattern Analysis and Machine Intelligence 11 (12) (1989) 1310–1312.
[13] O.D. Faugeras, Q.T. Luong, S.J. Maybank, Camera self-calibration: theory experiments, European Conference on Computer Vision (1992) 321–334.

[14] R.I. Hartley, Kruppa's equations derived from the fundamental matrix, Pattern Analysis and Machine Intelligence 19 (2) (1997) 133–135.
[15] O.D. Faugeras, What can be seen in three dimensions with an uncalibrated stereo ring?, European Conference on Computer Vision 588 (1992) 563–578.
[16] R. Hartley, R. Gupta, T. Chang, Stereo from uncalibrated cameras, Computer Vision and Pattern Recognition (1992) 761–764.
[17] R.I. Hartley, Estimation of relative camera position for uncalibrated cameras, European Conference on Computer Vision (1992) 579–587.
[18] R. Deriche, Z. Zhang, Q.-T. Luong, O. Faugeras, Robust recovery of the epipolar geometry for an uncalibrated stereo ring, European Conference on Computer Vision 800 (1994) 567–576.
[19] R.I. Hartley, Self-calibration from multiple views with a rotating camera, European Conference on Computer Vision 800 (1994) 471–478.
[20] M. Li, Camera calibration of a head-eye system for active vision, European Conference on Computer Vision 800 (1994) 543–554.
[21] Q.-T. Luong, T. Viéville, Canonic representation for geometries of multiple projective views, European Conference on Computer Vision 800 (1994) 589–599.
[22] Q.-T. Luong, O.D. Faugeras, A stability analysis of the fundamental matrix, European Conference on Computer Vision 800 (1994) 577–588.
[23] M.J. Brooks, L. Agapito, D.Q. Huynh, L. Baumela, Direct Methods for Self-Calibration of a Moving Stereo Head, Fourth European Conference on Computer Vision, vol. 2, Cambridge, UK, 1996, pp. 415–426.
[24] J.-H. Jang, H. Ki-Sang, Self-Calibration of a Stereo-Camera by Pure Translational Motion, IEEE International Conference on Image Processing, vol. 2, Laussane, Switzerland, 1996, pp. 297–300.
[25] Z. Zhang, Q.-T. Luong, O. Faugcras, Motion of an uncalibrated stereo ring: self-calibration and metric reconstruction, IEEE Transactions on Robotics and Automation 12 (1) (1996) 103–113.
[26] Z. Zhang, Determining the epipolar geometry and its uncertainty: a review, International Journal of Computer Vision 27 (2) (1998) 161–198.
[27] P.H.S. Torr, D.W. Murray, The development and comparison of robust methods for estimating the fundamental matrix, International Journal of Computer Vision 24 (3) (1997) 271–300.
[28] F. Li, M. Brady, C. Wiles, Fast Computation to the Fundamental Matrix for Active Stereo Vision System, Fourth European Conference on Computer Vision, vol. 1, Cambridge, UK, 1996, pp. 157–166.
[29] P.J. Rousseeuw, A.M. Leroy, Robust Regression and Outlier Detection, Wiley, New York, 1987.
[30] M. Bober, N. Greorgis, J. Kittler, On accurate and robust estimation of fundamental matrix, Computer Vision and Image Understanding 72 (1) (1998) 39–53.
[31] C.V. Stewart, MINPRAN: a new robust estimator from computer vision, IEEE Transactions on Pattern Analysis and Machine Intelligence 17 (10) (1995) 925–938.
[32] P.H.S. Torr, A. Zisserman, MLESAC: a new robust estimator with application to estimating image geometry, Computer Vision and Image Understanding 78 (2000) 138–156.
[32] Q.-T. Luong, O.D. Faugeras, The fundamental matrix: theory, algorithms, and stability analysis, Intemational Journal of Computer Vision 17 (1) (1996) 43–75.
[34] J. Salvi, An approach to coded structured light to obtain three dimensional information, PhD Thesis, Universitat de Girona, Departament d'Electrònica, Informàtica i Automàtica, 1997.
[35] R. Hartley, A. Zisserman, Multiple View Geometry in Computer Vision, Cambridge University Press, London, 2000.
[36] W. Chojnacki, M.J. Brooks, D. Galwey, A. van den Hengel, A new approach to constrained parameter estimation applicable to some computer vision problems, Statistical Methods in Video Processing Workshop held in conjunction with ECCV'02, Copenhagen, Denmark, June 1–2, 2002.
[37] M.J. Brooks, W. Chojnacki, D. Gawley, A. van den Hengel, What value covariance information in estimating vision parameters?, in: I.C. Society (Ed.), Proceedings of the Eighth IEEE International Conference on Computer Vision, vol. 1, 2000, pp. 302–308.
[38] W. Chojnacki, M.J. Brooks, A. van den Hengel, D. Gawley, On the fitting of surfaces to data with covariances, IEEE Transactions on Pattern Analysis and Machine Intelligence 22 (11) (2000) 1294–1303.
[39] P.J. Huber, Robust Statistics, Wiley, New York, 1981.
[40] E. Mosteller, J. Turkey, Data and Analysis and Regression, Addison-Wesley, Reading, MA, 1977.
[41] P.H.S. Torr, Bayesian model estimation and selection for epipolar geometry and generic manifold fitting, International Journal of Computer Vision 50 (1) (2002) 35–61.
[42] R. Hartley, In defence of the 8-point algorithm, Proceedings of the Eighth International Conference on Computer Vision, IEEE Computer Society Press, Boston, 1995, pp. 1064–1070.
[43] Z. Zhang, R. Deriche, O. Faugeras, Q.-T. Luong, A robust technique for matching two uncalibrated images through the recovery of the unknown epipolar geometry, Technical Report 2273, Institut National de Recherche en Informatique et Automatique, May 1994.
[44] Z. Zhang, The matching problem: the state of the art, Technical Report 2146, Institut National de Recherche en Informatique et en Automatique, December 1993.
[45] G. Csurka, C. Zeller, Z. Zhang, O.D. Faugeras, Characterizing the uncertainty of the fundamental matrix, Computer Vision and Image Understanding 68 (1) (1997) 18–36.
[46] P.H.S. Torr, A. Zisserman, Robust detection of degenerate configurations while estimating the fundamental matrix, Computer Vision and Image Understanding 71 (3) (1998) 312–333.
[47] Z. Zhang, On the epipolar geometry between two images with lens distortion, International Conference on Pattern Recognition 1 (1996) 407–411.